POLITECNICO DI TORINO
Repository ISTITUZIONALE

Separating ^{39}Ar from ^{40}Ar by cryogenic distillation with Aria for dark matter searches

Original
Separating ^{39}Ar from ^{40}Ar by cryogenic distillation with Aria for dark matter searches / Collaboration, Darkside; Agnes, P.; Albergo, S.; Albuquerque, I. F. M.; Alexander, T.; Alici, A.; Alton, A. K.; Amaudruz, P.; Arba, M.; Arpaia, P.; Arcelli, S.; Ave, M.; Avetissov, I. Ch.; Avetisov, R. I.; Azzolini, O.; Back, H. O.; Balmforth, Z.; Barbarian, V.; Barrado Olmedo, A.; Barrillon, P.; Basco, A.; Batignani, G.; Bondar, A.; Bonivento, W. M.; Borisova, E.; Bottino, B.; Boulay, M. G.; Buccino, G.; Bussino, S.; Busto, J.; Buzulutskov, A.; Cadeddu, M.; Cadoni, M.; Caminata, A.; Canesi, E. V.; Canci, N.; Cappello, G.; Caravati, M.; C., M.; Cargioli, N.; Carlini, M.; Carnesecchi, F.; Castello, P.; Castellani, A.; Catalanotti, S.; Cataudella, V.; Cavalcante, P.; Cavuoti, S.; Cebrian, S.; Cela Ruiz, J. M.; Celano, B.; Chashin, S.; Chepurnov, A.; Cicalò, C.; Cifarelli, L.; Cintas, D.; Coccetti, F.; Cocco, V.; Colocci, M.; Conde Vilda, E.; Consiglio, L.; Copello, S.; Corning, J.; Covone, G.; Czudak, P.; D'Aniello, M.; D'Auria, S.; Da Rocha Rolo, M. D.; Dadoun, O.; Daniel, M.; Davini, S.; De Candia, A.; De Cecco, S.; De Falco, A.; De Filippis, G.; De Gruttola, D.; De Guido, G.; De Rosa, G.; Della Valle, M.; Dellacasa, G.; De Pasquale, S.; Derbin, A. V.; Devoto, A.; Di Noto, L.; Di Eusanio, F.; Dionisi, C.; Di Stefano, P.; Dolganov, G.; Dongiovanni, D.; Dordei, F.; Downing, M.; Erjavec, T.; Falciano, S.; Farenzena, S.; Fernandez Diaz, M.; Filip, C.; Fiorillo, G.; Franceschi, A.; Franco, D.; Frolov, E.; Funicello, N.; Gabriele, F.; Galbiati, C.; Garbini, M.; Garcia Abia, P.; Gendotti, A.; Ghiano, C.; Giampaolo, R. A.; Giganti, C.; Giorgi, M. A.; Giovanetti, G. K.; Gligan, M. L.; Goicoechea Casanueva, V.; Gola, A.; Goretti, A. M.; Graciani Diaz, R.; Grigoriev, G. Y.; Grobov, A.; Gromov, M.; Guan, M.; Guerzoni, M.; Guetti, M.; Gulino, M.; Guo, C.; Hackett, B. R.; Hallin, A.; Haranczyk, M.; Hill, S.; Horikawa, S.; Hubaut, F.; Hugues, T.; Hungerford, E. V.; Ianni, An.; Ippolito, V.; James, C. C.; Jillings, C.; Kachru, P.; Kemp, A. A.; Kendziora, C. L.; Keppel, G.; Khomyakov, A. V.; Kim, S.; Kish, A.; Kochanek, I.; Kondo, K.; Korga, G.; Kubankin, A.; Kugathasan, R.; Kuss, M.; Kuzniak, M.; La Commara, M.; La Delfa, L.; Lai, M.; Lami, N.; Langrock, S.; Leyton, M.; Li, X.; Lidey, L.; Lippi, F.; Lissia, M.; Longo, G.; Maccioni, N.; Machulin, I. N.; Mapelli, L.; Marasciulli, A.; Margotti, A.; Mari, S. M.; Maricic, J.; Marinelli, M.; Mart, M.; Martinez Rojas, A. D.; Martini, A.; Martoff, C. J.; Mascia, M.; Masetto, M.; Masoni, A.; Mazzi, A.; Mcdonald, A. B.; Mclaughlin, J.; Messina, A.; Meyers, P. D.; Miletic, T.; Milincic, R.; Miola, R.; Moggi, A.; Moharana, A.; Moioli, S.; Monroe, J.; Morisi, S.; Morrocchi, M.; Mozhevitina, E. N.; Mr, T.; Muratova, V. N.; Murenu, A.; Muscas, C.; Musenich, L.; Musico, P.; Nania, R.; Napolitano, T.; Navrer Agasson, A.; Nessi, M.; Nikulin, I.; Nowak, J.; Oleinik, A.; Oleynikov, V.; Pagani, L.; Pallavicini, M.; Palmas, S.; Pandola, L.; Pantic, E.; Paoloni, E.; Paternoster, G.; Pegoraro, P. A.; Pellegrini, L. A.; Pellegrino, C.; Pelczar, K.; Perotti, F.; Pesudo, V.; Picciau, E.; Pietropaolo, F.; Pinna, T.; Pocar, A.; Podda, P.; Poehlmann, D. M.; Pordes, S.; Poudel, S. S.; Pralavorio, P.; Price, D.; Raffaelli, F.; Ragusa, F.; Ramirez, A.; Razeti, M.; Razeto, A.; Renshaw, A. L.; Rescia, S.; Rescigno, M.; Resnati, F.; Retiere, F.; Rignanese, L. P.; Ripoli, C.; Rivetti, A.; Rode, J.; Romero, L.; Rossi, M.; Rubbia, A.; Rucaj, M.; Sabiu, G. M.; Salatino, P.; Samoylov, O.; S., E.; Sandford, E.; Sanfilippo, S.; Sangiorgio, V. A.; Santacroce, V.; Santone, D.; Santorelli, R.; Santucci, A.; Savarese, C.; Scapparone, E.; Schlitzer, B.; Scioli, G.; Semenov, D. A.; Shaw, B.; Shchagin, A.; Sheshukov, A.; Simeone, M.; Skensved, P.; Skorokhvatov, M. D.; Smirnov, O.; Smith, B.; Sokolov, A.; Stefanizzi, R.; Steri, A.; Stracka, S.; Strickland, V.; Stringer, M.; Sulis, S.; Suvorov, Y.; Szelc, A. M.; Zsücs-Balázs, J. Z.; Tartaglia, R.; Testera, G.; Thorpe, T. N.; Tonazzo, A.; Torres-Lara, S.; Tosti, S.; Tricomi, A.; Tuveri, M.; Unzhakov, E. V.; Usai, G.; Vallivilayil John, T.; Vescovi, S.; Viant, T.; Viel, S.; Vishneva, A.; Vogelaar, R. B.; Wada, M.; Wang, H.; Wang, Y.; Westerdale, S.; Wheadon, R. J.; Williams, L.; Wojcik, Ma. M.; Wojcik, Ma.; Xiao, X.; Yang, C.; Zani, A.; Zenobio, F.; Zichichi, A.; Zuzel, G.; Zykova, M. P.. - In: EUROPEAN PHYSICAL

Availability:
This version is available at: 11583/2872412 since: 2021-02-24T18:28:46Z

Publisher:
Springer

Published
DOI:10.1140/epjc/s10052-021-09121-9

Terms of use:
This article is made available under terms and conditions as specified in the corresponding bibliographic description in the repository

Publisher copyright
GENERICO preprint/submitted version accettata

This article has been accepted for publication in EUROPEAN PHYSICAL JOURNAL. C, PARTICLES AND FIELDS, published by Springer.

(Article begins on next page)

07 May 2026

JOURNAL. C, PARTICLES AND FIELDS. - ISSN 1434-6052. - ELETTRONICO. - 81:359(2021). [10.1140/epjc/s10052-021-09121-9]

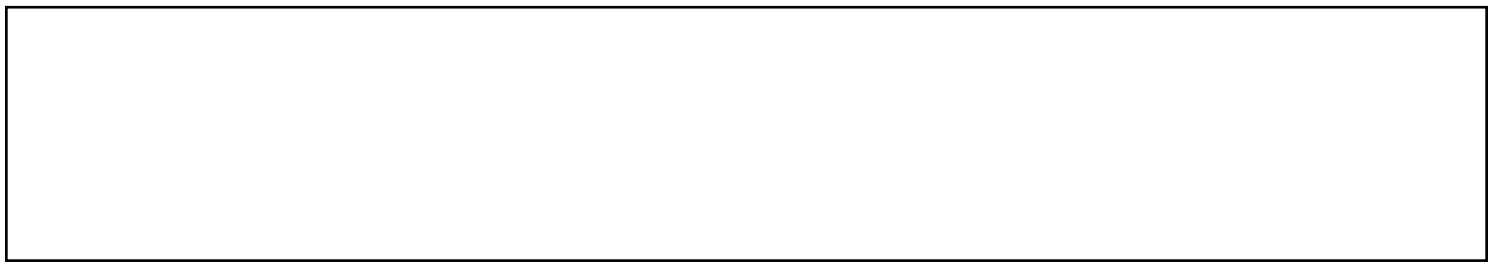

07 May 2026

Eur. Phys. J. C manuscript No.
(will be inserted by the editor)

Separating ^{39}Ar from ^{40}Ar by cryogenic distillation with Aria

The DarkSide-20k Collaboration[a,1]

[1]See back for author list

January 18, 2021

Abstract The Aria project consists of a plant, hosting a 350 m cryogenic isotopic distillation column, the tallest ever built, which is currently in the installation phase in a mine shaft at Carbosulcis S.p.A., Nuraxi-Figus (SU), Italy. Aria is one of the pillars of the argon dark-matter search experimental program, lead by the Global Argon Dark Matter Collaboration. Aria was designed to reduce the isotopic abundance of ^{39}Ar, a β-emitter of cosmogenic origin, whose activity poses background and pile-up concerns in the detectors, in the argon used for the dark-matter searches, the so-called Underground Argon (UAr). In this paper, we discuss the requirements, design, construction, tests, and projected performance of the plant for the isotopic cryogenic distillation of argon. We also present the successful results of isotopic cryogenic distillation of nitrogen with a prototype plant, operating the column at total reflux.

1 Introduction

Large liquid argon detectors offer one of the best avenues for detecting galactic Weakly Interacting Massive Particles (WIMPs) via their scattering on atomic nuclei. However, atmospheric argon (AAr) has a naturally occurring radioactive isotope, ^{39}Ar, of isotopic abundance of 8×10^{-16} in mass, which is a β-emitter of cosmogenic origin, and whose activity of about 1 Bq/kg raises background and pile-up concerns. Indeed, the liquid argon target allows for powerful discrimination between nuclear and electron recoil scintillation signals via pulse-shape discrimination [1–3], provided the background rate is not too high. However, this discrimination method cannot be applied in experiments that look at the ionization signal only [4, 5]. The use of argon extracted from underground wells, the so-called Underground Argon (UAr), with a highly suppressed content of ^{39}Ar, is therefore pivotal for the physics potential of dark matter search experiments.

The DarkSide-50 experiment, a liquid argon time projection chamber (LAr TPC) at Laboratori Nazionali del Gran Sasso (LNGS), used a 150 kg active mass of UAr extracted from CO_2 wells in Cortez, CO, USA, and measured the ^{39}Ar Depletion Factor (DF) with respect to AAr to be 1400 ± 200 [2]. A new production chain, that was recently set up to significantly increase the production of UAr. This new production needs to meet the target requirements of the Global Argon Dark Matter Collaboration (GADMC), a worldwide effort that unifies the DarkSide, DEAP-3600, MiniCLEAN, and ArDM experimental groups, for the construction of new experiments for argon dark-matter searches. In order of increasing size, these new experiments are a potential DarkSideLowMass, with approximately 1 t target, optimized for the detection of low-mass dark matter, aiming at improving the world-leading results of the DarkSide-50 experiment [4, 5], the 51.1 t target mass DarkSide-20k [6], under construction at LNGS, Italy, and the prospected Argo, of 400 t target mass, that will push the experimental sensitivity down to the so-called neutrino floor. The argon procurement for this new production chain starts from the Urania plant, now in the construction phase in Cortez, CO, USA, that will extract and purify UAr at a maximum production rate of about 330 kg/d. The ^{39}Ar radioactivity of UAr, though remarkably lower than that of AAr, is neither low enough for the needs of the DarkSide-LowMass experiment, where it would be the limiting background to the cross-section sensitivity, nor for the Argo experiment, where it would cause a major event pile-up, if built with the double-phase TPC technology.

The cryogenic isotopic distillation plant Aria, which is currently in the installation phase in a mine shaft at Carbo-Sulcis S.p.A., in Nuraxi-Figus (SU), Italy, was designed to further reduce the ^{39}Ar isotopic fraction of the UAr by an-

[a]e-mail: ds-ed@lngs.infn.it

other factor of 10 per pass, with a production rate of several kg/d. While the 350 m tall, 31.8 cm inner diameter, distillation column under construction fits the needs of DarkSide-LowMass in terms of production rate, for the larger Argo experiment a new wider column would need to be built.

Cryogenic isotopic distillation with rectifying columns is a well established technique [7] and has received quite some attention in the context of the stable isotope separation of the main biogenic elements such as carbon and oxygen and some industrial-scale plants have already been built. However, for argon isotopic distillation, this is the first time that such a plant is proposed and constructed. In addition to cryogenic distillation, a few other techniques are currently available for the separation of argon isotopes, based on the difference in molecular mass, such as centrifugal separation and diffusion separation, the latter based on the different average speed, at thermal equilibrium, among isotopes of the same energy. However, their application is limited by the low yield and the high cost per unit mass of separated isotopes. As a matter of fact, the cryogenic isotopic distillation plant Aria appears as a very promising new avenue for the depletion from ^{39}Ar of such large quantities of argon, at reasonable cost and time. It is interesting to note that target purification via distillation, though not isotopic, with cryogenic columns in the context of dark matter search detectors was also pursued by other collaborations using xenon [8–11].

The technological capability to achieve efficient isotopic separation with cryogenic distillation allows to widen the application of the Aria project to other fields, where the production of stable isotopes is required, such as e.g. in medical applications. However, in this paper we will focus on the application of the Aria plant to the isotopic distillation of argon.

A very important achievement for this project was a nitrogen distillation run of the prototype plant, a short version of the Aria column using only the reboiler, the condenser and one central module, together with all the auxiliary equipment of the full column, installed in a surface building. The successful outcome of this run paved the way to the continuation of the project and the construction of the full plant.

2 Design requirements

Isotopic separation by cryogenic distillation exploits the relative volatility of different isotopes, namely, for ideal mixtures, the ratio of their vapor pressures at a given temperature. Continuous distillation, with a large number of distillation stages, where the liquid and vapor phases undergo a countercurrent exchange at thermodynamic equilibrium, is used to optimize the separation of isotopes that have relative volatility close to unity. As detailed in Sect. 3, heat is constantly provided from a bottom heat exchanger, in the so-called *reboiler*, that vaporizes the liquid, and extracted from a top heat exchanger, in the so-called *condenser*, that condenses the vapor. To perform the isotopic separation, the column temperature ranges between the boiling point of ^{40}Ar (bottom) and of ^{39}Ar (top) at the operating pressure, slightly above 1 bar. The pre-cooled UAr feed enters the column at a given height and flow. The vapor rises in the column and re-condenses, while the liquid sinks by gravity and then reboils. In the rectifying section (above the feed point), the molar fraction of ^{39}Ar is larger than in the feed argon, while in the stripping section (below the feed point) it is smaller than in the feed argon. Liquid argon depleted of ^{39}Ar is then collected continuously from the bottom of the column, whereas argon enriched of ^{39}Ar is collected from the top. Since the ^{39}Ar has a very low isotopic fraction even in atmospheric argon, its volatility relative to the other argon isotopes was never measured. Therefore, for the column design, the relative volatility of ^{39}Ar to ^{40}Ar, or its more commonly used natural logarithm, $\ln(\alpha_{39-40})$, was derived from the measured relative volatility of ^{36}Ar to ^{40}Ar, which is 0.0060 ± 0.0001 [12], at the mean operating temperature of the column of 89.5 K, as shown in Sect. 3. According to the model of [13], the dependence of $\ln(\alpha_{A-40})$ on the isotopic mass A is $\ln(\alpha_{A-40}) \propto (40-A)/A$. This means that, at 89.5 K, $\ln(\alpha_{39-40})$ is about 0.0014 and α_{39-40} is about 1.0014, which is the value assumed for all the calculations in this paper. The uncertainty coming from model extrapolation is however difficult to estimate and therefore this number should be taken as an approximate value. The temperature dependence of α_{39-40} turns out to be about -0.00005/K.

The relative volatility of two species provides an estimate of how difficult it is to separate two species. Since this ratio is close to 1 for ^{39}Ar and ^{40}Ar, the separation is expected to be very difficult. To optimize the distillation process, the Aria column makes use of a high performance packing material instead of the distillation trays. The two related quantities that characterize the separation capability of distillation columns are the number of equivalent theoretical trays, N_T, (in a distillation columns the N theoretical stages consist of the N_T theoretical trays with the eventual addition of the reboiler and the condenser, in the case they represent equilibrium stages) and the Height Equivalent to a Theoretical Plate, HETP, the product of the two yielding the total column height.

In the Aria distillation column, for a binary mixture, the minimum number of theoretical stages needed, N_{min}, at total reflux is given by the Fenske equation [14]:

$$N_{\min} = \frac{\ln(S^0_{39-40})}{\ln(\alpha_{39-40})}, \tag{1}$$

for a separation, S^0_{39-40}:

$$S^0_{39-40} = \frac{x_D}{1-x_D}\frac{1-x_B}{x_B} \sim \frac{x_D}{x_B}, \quad (2)$$

where x_D is the molar fraction of ^{39}Ar in the top, x_B the molar fraction of ^{39}Ar in the bottom, and $x_D, x_B \ll 1$.

Requiring for instance a separation of 10, from eq. (1) it follows that N_{min}=1645. Moreover, when the column operates in finite reflux mode, the number of required stages is larger than N_{min}. To include such a large number of stages, the column needs to be very tall and be filled with high performance packing, i.e. with a small HETP. Moreover, for efficient use of the packing, there is a limitation on the liquid flow per unit area, usually specified by the vendor. Therefore not only the height but also the diameter matters for sizeable distillate production.

To support such a tall column, a convenient and cheap solution was found with its installation in an underground vertical mineshaft of 5 m diameter and 350 m depth, dug in the 1940s, which was made available to Aria by the end of the mine coal extraction cycle, at the end of 2018.

The first phase of the Aria project, which is the subject of this paper, consists of a column of internal diameter d=31.8 cm, with 3 mm wall thickness, enclosed in a vacuum cold box of 71.1 cm diameter, with a total height approximately equal to the mineshaft depth. The support structure of the column in the shaft is designed in a way to allow for the installation at later times of a wider column with a maximum cold box diameter of 2.0 m.

The rest of the paper is organized as follows. In Sect. 3 we discuss the plant design, followed by a description of the column in Sect. 4. In Sect. 5 we present the column vacuum leak tests. In Sect. 6 we discuss the prototype tests and the validation of some characteristics of the plant with measurements, and in Sect. 7 the projected performance of Aria for argon isotopic distillation.

3 Plant design

The Aria plant simplified scheme is displayed in Fig. 1. The column, cryogenic tanks, and heat exchangers are enclosed in a cold box (grayed area) which is vacuum-tight and designed to reduce thermal losses. The cryogenic circuit of the plant is designed with two independent loops: the argon loop (dark green lines for the liquid and light green lines for the vapor/gas) and the refrigeration loop, with nitrogen gas (cyan lines) and liquid (dark blue lines) that are used to evaporate and to condense the argon. The Aria plant was designed in a way that minimizes nitrogen consumption and optimizes energy efficiency, by using a closed-loop refrigeration circuit and appropriate use of heat exchangers.

UAr will be transported from the Urania plant being constructed in Cortez, Colorado, USA, to Aria in Sardinia, Italy, and then from Aria to LNGS, Italy, inside gas skids. The argon gas from the Feed Skid is fed into the distillation column through a flow controller, and pressure-regulated to about 1 bar. A heat exchanger (HE4) with the output distillate stream is used to cool the argon. The bottom stream comes out of the column as a liquid, gets heated as it passes through an air heater (H1), compressed (C1) and then delivered to the Bottom Skid. This is the argon that will be used in the experiments. At the top of the column, the distillate stream, enriched in ^{39}Ar, is delivered to the Distillate Storage after passing through HE4 and a compressor (C2).

Liquid nitrogen is used as cooling fluid in the heat exchanger (HE1) of the column condenser. The nitrogen vapor from the output of HE1 is heated through the heat exchanger HE2 and then compressed, by a screw rotary compressor (C3), to a pressure value between 2 bar and 4 bar. The compressed gas, after cooling in HE2, is used as heating fluid in the heat exchanger (HE3) of the reboiler. The liquefied nitrogen, after passing through a nitrogen phase separator tank (BT), is pumped by a modular reciprocating pump (P1), with a delivery pressure up to 100 bar, all the way up to the top of the column, and fed back to HE1. Liquid nitrogen is stored and fed into the circuit from an external 50 m^3 tank. The excess nitrogen gas from the system is fed back to the tank, after being liquefied by four 4 kW cryogenerators (Stirling Cryogenics), inherited from the ICARUS experiment at LNGS.

Brazed plate heat exchangers are used for the reboiler (HE3), the condenser (HE1), and HE2. These heat exchangers are characterized by high heat transfer efficiency and limited size and are the ideal solution for this application. Coil heat exchangers (H1 and HE4) are used for the inlet and outlet argon flows.

Fig. 1 reports also the values of operating pressure and temperature, for ^{39}Ar-^{40}Ar distillation, obtained with a plant engineering simulation using the Aspen HYSYS package. It can be seen that the column operating temperature varies from the top to the bottom between 87.8 K and 90.9 K.

4 Column and cold box structure

For construction and transport, both the column and the surrounding cold box have a modular structure. The thirty modules were assembled at the production site. The 28 central modules are identical cylindrical elements about 12 m tall, with a 71.1 cm diameter and an approximate weight of 3 t. The top module, about 9.5 m tall and 1.2 m diameter, hosts the top of the distillation column, about 1 m high, the condenser (HE1), a liquid nitrogen buffer tank, not shown in the simplified scheme of Fig. 1, and two heat recovery exchangers (HE4 and HE2). The bottom module, about 4 m tall and 1.5 m diameter, hosts the bottom of the distillation column,

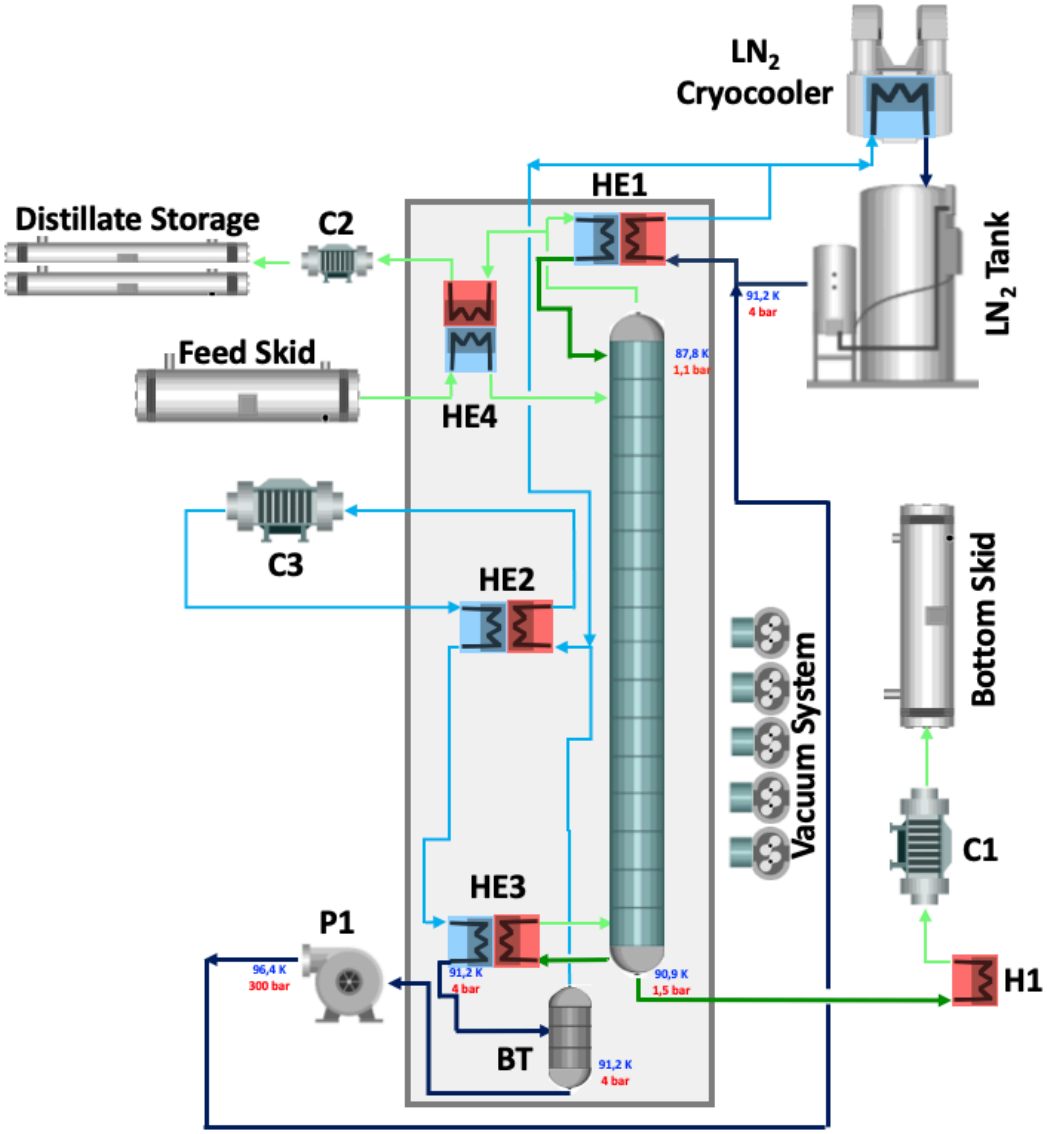

Fig. 1 Simplified scheme of the Aria plant. The full description can be found in the text. The color-coding of the heat exchangers is such that the red section provides heat to the fluid while the blue section removes heat from it. The scheme also reports the values of operating pressure and temperature for ^{39}Ar-^{40}Ar distillation, as obtained from a plant engineering simulation (Aspen - HYSYS).

about 1 m high, the reboiler (HE3), and a nitrogen phase separator tank (BT). Fig. 2 shows some of the central modules stored at the Carbosulcis site, ready for installation in the shaft. Fig. 3 displays the top module while Fig. 4 shows the bottom module.

The structure of the cold box, the internal equipment, and the piping are fully welded to reduce the risk of leaks. All weldings were performed at the manufacturing company where the modules were assembled, except for the orbital welds between modules, which will be performed in the mineshaft.

To account for the thermal contraction of the structure, axial bellows are interleaved between every other module. At cold, the bellows expands by about 3 cm. Due to the presence of bellows, the support of each module is independent from the others. The load is distributed laterally to the shaft walls. Every module is supplied with anchor points, whose sizing takes into consideration both the static weight and the stresses due to the cold box operating pressure. The anchor points are bolted to a structure, discussed in Sect. 4.3, which is fixed to the lateral wall of the shaft.

4.1 Internal structure

The 28 central modules are filled with a structured stainless steel packing (Sulzer CY gauze). To stay below the flooding limit and, therefore, guarantee an efficient distillation with this packing, according to measurements per-

Fig. 2 The central modules of the column stored at Carbosulcis S.p.A., Nuraxi-Figus site, ready for installation.

Fig. 3 The top module of the column.

Fig. 4 The bottom module of the column.

formed by the vendor with chlorobenzene/etilbenzene mixtures, a maximum specific liquid volume flow rate or load, $\hat{V}_L$, of $5\,\mathrm{m}^3/(\mathrm{h\,m}^2)$, is allowed. Given the column inner diameter of 31.8 cm, this corresponds to a liquid volume flow rate, V_L, of $0.4\,\mathrm{m}^3/\mathrm{h}$ or to a mass flow rate of $560\,\mathrm{kg/h}$. With this load and at the average operating pressure of the column with argon, the sizing parameter for packed columns F, defined as $U_V \cdot \sqrt{\rho_V}$, where U_V is the superficial gas velocity, i.e. the vapor volume flow rate, V_V, per unit column cross section, and ρ_V the vapor argon density at equilibrium, whose value for argon is given in Table 1, is $0.8\,\sqrt{\mathrm{Pa}}$. With this value of F, from the reference curves provided by the packing producer (Sulzer) and approximating to atmospheric pressure, one would expect an HETP of about 10 cm and a pressure drop of $0.7\,\mathrm{mbar/m}$. The measurement of these parameters in the cryogenic environment is an essential step of this research, and is the main focus of the tests described in Sect. 6. To avoid the channeling of the fluid in the packing and to optimize the uniformity across the column section, each module is divided into four subsections of packing, with an active height of 2.56 m each, interleaved with a liquid distributor, shown in Fig. 5. The liquid formed on the distributor plate is streamed, through holes located at 3 cm height in perforated pipes uniformly distributed along the plate surface, to the packing section below. The vapor rises towards the packing section above through 12.5 cm high chimneys. The total active height of the column is about 287 m, that corresponds to a N of 2870. The pressure drop along the column is about 0.7 bar, with 0.5 bar due to the distributors. The minimum argon mass that needs to be in the column for efficient distillation, is largely dominated by the liquid component, the vapor contributing only to 5 % of the total. The two major contributions come from the distributors, $0.3\,\mathrm{m}^3$, and from the wetting of the packing, the so called holdup, $1.1\,\mathrm{m}^3$. The packing wettability was assumed for this calculation to be 5 %, as specified by the packing vendor. Again, its value was given for the above mentioned organic mixture and, therefore, will need to be verified at the cryogenic temperatures of the column with argon. The total argon mass in the column during distillation, with the above mentioned assumptions, turns out to be approximately 2.5 t.

Fig. 5 A view from above of a liquid distributor.

The thermal load of the column was calculated assuming the maximum liquid flow specified by the packing producer, as discussed in Sect. 4. The required thermal duty for the cryogenic system turns out about 25 kW, broadly given by the maximum liquid flow times the heat of vaporisation. The

total electric power needed for the plant operation is about 500 kW, including the cryocooler, compressors, fluid, and vacuum system pumps load.

4.2 Thermal insulation

To minimize heat transfer through conduction and radiation from the environment to the cryogenic distillation column, a 10^{-5} mbar vacuum is made in the cold box. In order to maintain the desired vacuum level, several pump stations of total pumping speed 10^4 L/s, are installed along the column. In addition, 20 layers of Multi-Layer Insulation (MLI) are wrapped around the column, and 10 are wrapped around all the other lines and reservoirs within the col box. With this insulation, the residual thermal radiation input power to the column is about 1 W/m^2, a few percent of the thermal duty cycle of the column. Insulation is also provided on the equipment and piping outside of the cold box, for minimizing heat losses and for personal protection against the risk of injuries by accidental contacts. For cold points, the insulation is based on synthetic rubber, covered with aluminum sheets. Vacuum jacketed pipes are used for long-distance connections.

4.3 Support structure in the shaft

The support structure of the column is made of austenitic steel and is assembled by bolted connections. It is made of discrete structures, shown in Fig. 6, spaced in the vertical direction by 4 m. To keep a safety margin, three supporting structures per central module are foreseen, each one able, in principle, to hold the module independently. The anchoring shelves penetrate the rock up to an average depth of about 120 cm for the central support, and 80 cm for the other two. For filling the 300 mm openings, a cement based thixotropic mortar is used, with high mechanical strength and compensated shrinkage. Fig. 7 shows the installation of the first support structure in the well. Load tests were performed applying a 3 t load and no significant deflection was observed.

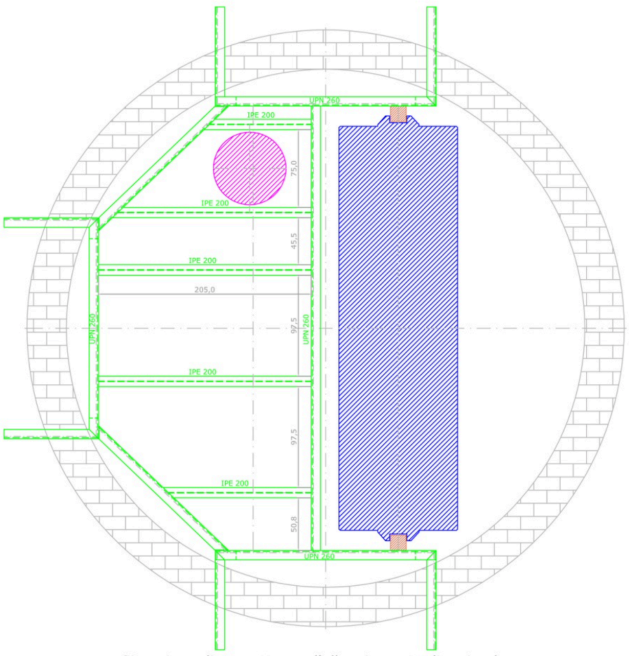

Fig. 6 Horizontal cut of the mineshaft showing the stainless steel structure, in green, for positioning the column, in magenta. The blue rectangle on the right is the elevator.

5 Vacuum leak tests of individual modules

Leak detection is a critical step in the construction of Aria, since its functioning depends on a high cold box insulating vacuum and the distillation process should not be contaminated from air. For that reason, by the way, the pressure of the process column and related lines is kept above the atmospheric pressure. The leak-check procedure has to be quite strict, in particular for those lines that will undergo thermal stresses. Indeed, the column and the service lines will go back and forth from room temperature down to liquid argon/nitrogen temperatures several times during their lifetime.

An upper limit of 10^{-9} mbarL/s was set on the leak rate for each leak check performed on single modules during testing, mainly on welds. Each column segment was tested twice. The first phase of tests took place at the manufacturing company site (Polaris Engineering), where the column and the service lines were fully tested, before wrapping them around with MLI. The second phase of the leak checks, carried out at CERN, CH, included also a full check of the cold box and bellows. For the tests, each module was closed temporarily with end-caps, the space between the cold box and the distillation column was evacuated with a turbopump system, and the column and the service lines were filled with a mixture of 90% of air and 10% of helium. In this way, the potential leak can be found by the leak detector associated with the turbopump system. All the modules were validated in a two-step approach to confirm a leak rate smaller than 10^{-9} mbarL/s on each module. Since there are 30 column segments in total, the total leak rate is expected to be smaller

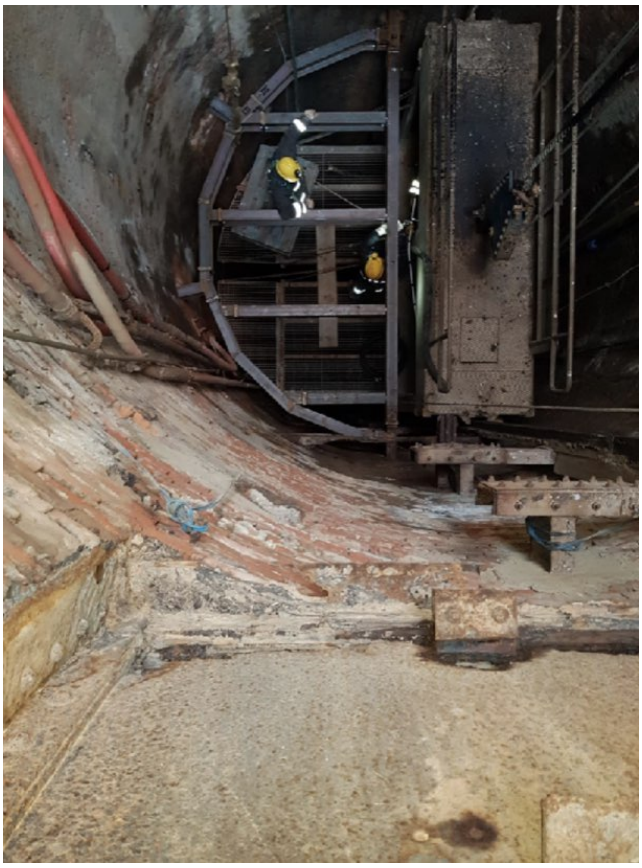

Fig. 7 Installation of the first support structure in the shaft of the Carbosulcis mine, Seruci site.

than 3×10^{-7} mbar L/s at room temperature. An additional one-off leak test was performed at CERN to validate module tightness after a thermal cycle down to 87 K. The reboiler unit was chosen for this test, due to its complex internal weld configuration, and tightness below 10^{-9} mbar L/s was again confirmed.

6 Performance test at total reflux with a prototype column.

To verify the theoretical calculations about the distillation performance, and test the mechanical and cryogenic infrastructure prior to column installation in the mineshaft, a prototype plant was built in a surface building.

6.1 Prototype construction

The prototype plant is a short version of the Aria column using only the reboiler, the condenser and one central module, for a total height of 26 m, together with the auxiliary equipment, which is the same as that of the full column. It is located in the Laveria building of the Carbosulcis mine, Nuraxi-Figus site, as shown in Fig. 8 and Fig. 9. The mechanical support, made of galvanized and cold-painted carbon steel, consists of a square base structure with four feet of concrete and a modular iron pillar structure equipped on each side with two diagonal support beams. The structure includes seven level platforms, to allow the presence of operators along the column height. Though self-supporting, for additional safety, the support is fixed to the building structure at two different heights.

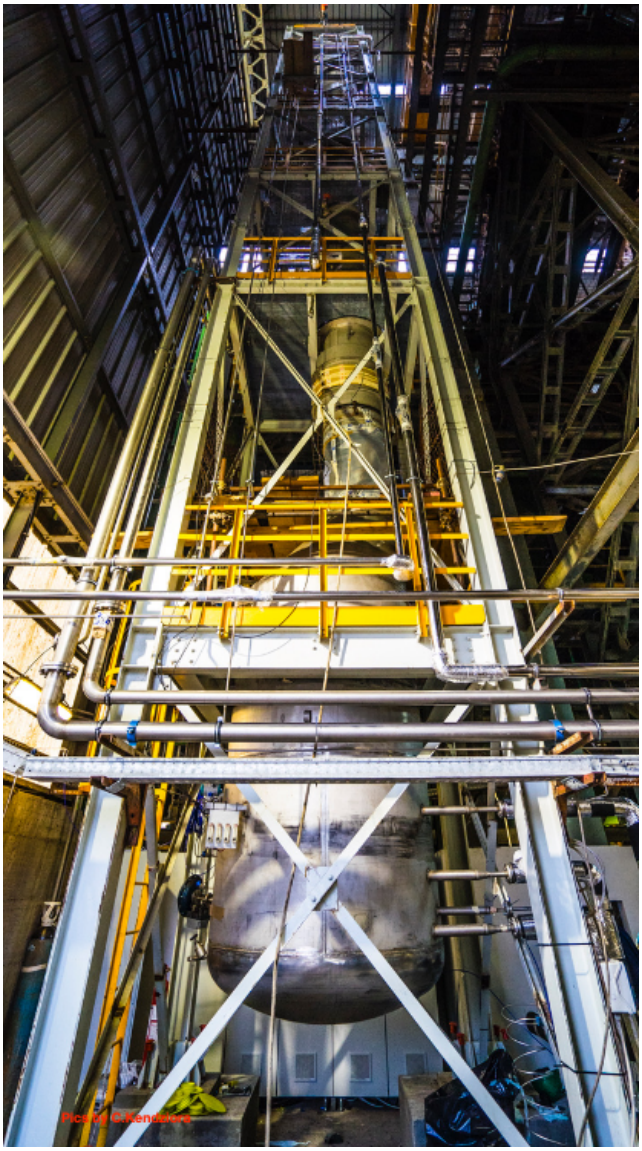

Fig. 8 The prototype Aria plant in the Laveria building of the Carbosulcis mine, Nuraxi-Figus site, viewed from the basis of the column.

After welding together the three modules, the column and the four service lines were leak checked with a calibrated leak detector. An external calibration leak was used to estimate the helium diffusion time along all the lines. This

Fig. 9 Aerial view of the prototype Aria plant located in the Laveria building of the Carbosulcis mine, Nuraxi-Figus site. From bottom left, clockwise, the liquid pumps, the cryocoolers and the gas compressor.

turned out to be between four and twenty seconds, depending on the line. Therefore it was decided to wait at least two minutes between every leak check to make sure that a possible signal could be associated with the precise tested weld. The standard technique of filling sealed bags with helium around the welds was used for all the procedure. The helium bags, once filled with helium, were not removed until the last leak check. Using this method an upper limit of 10^{-9} mbar L/s was set on all the welds between the modules.

Leak detection will become increasingly more difficult during the assembly of the modules in the shaft. With the leak test procedure just described, the increased size of the column, as the modules are assembled together, will cause a much longer response time of the leak detection system, reducing its sensitivity. To overcome this difficulty, the use of some new tools is foreseen. Devices called clamshells, developed at CERN, will surround the welds and create a small sealed space that can be quickly evacuated. Helium will flow inside the tube/column, and the potential leak in the weld can be therefore detected with a very fast response time.

6.2 Prototype Operation

For the commissioning of the prototype plant, different purity grades of N_2 were used both in the auxiliary circuit for cooling, and in the process circuit for the distillation inside the column. The operating parameters of the auxiliary system were about the same as those discussed in Sect. 3.

A dedicated slow-control system monitors and controls the distillation process and ll equipment in real time. This system uses LabVIEW (NI) as system-design platform and development environment, and it is organized with a distributed layered architecture. The control cabinets are interconnected by a private WLAN network, inside the Carbo-Sulcis network, with a Real Time Controller (NI cRIO 9039) reading out the data of the different expansion chassis (NI 9049) distributed over the network. In addition, PROFIBUS, a standard for fieldbus communication in automation technology, is integrated into the system to control third party equipment such as compressors, vacuum gauges and vacuum pumps. The slow control also features advanced controls such as Proportional Integral Derivative control, cascade control, threshold logic, interlocks over valves, inverters, and temperature controllers. Historical data are stored in a relational data base (PostgreSQL).

Plant operation started with feeding the cooling liquid nitrogen to the auxiliary circuit from the external storage tank and nitrogen of purity grade 5 into the column. Eight hours were needed to reach the target temperature. The total amount of nitrogen filling the column was estimated by taking into account that it was stored in 16 gas bottles of 50 L each, with an initial pressure of 200 bar and a final pressure of 80 bar. Using the Peng-Robinson equation of state, the total mass is then 110 kg.

The measurements reported in this paper refer to two distillation runs of the plant, 165 h in total, with two different screw-rotary compressor (C3) settings, with the column operated at total reflux. The two runs started and stopped with switching on and off the compressor and, with some delay, the pumps. Fig. 10 and Fig. 11 show the measured pressure vs. time and mass flow vs. time in the auxiliary system, downstream of the compressor. For these first two runs, an automated feedback system, foreseen in the plant design, regulating the flow downstream of the compressor, was not used. The auxiliary system gas pressure and flow stability were guaranteed only regulating by hand a bypass valve between the compressor and the gas flow meter. A better stability was reached during the second run, where fluctuations were limited to ± 0.3 bar and $\pm 20\,\mathrm{m}^3/\mathrm{h}$, as shown in Fig. 10 and Fig. 11, respectively. The pressure inside the column was measured by digital pressure transmitters with diaphragm seal measuring cell, located respectively below the first distributor from the top and right above the reboiler. Fig. 12 shows the measured pressure inside the column in

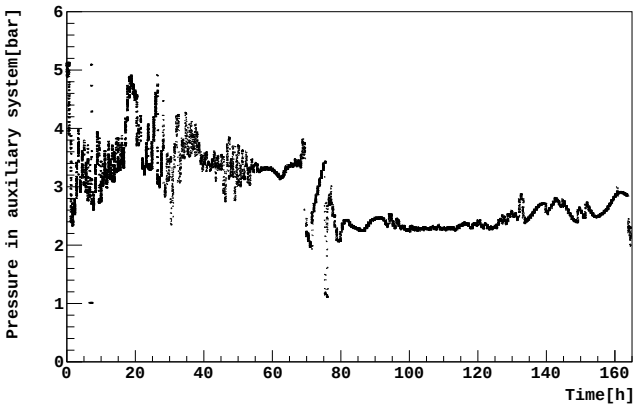

Fig. 10 Measured pressure in the auxiliary system downstream of the compressor vs time, for $^{29}N_2$-$^{28}N_2$ distillation in the prototype plant.

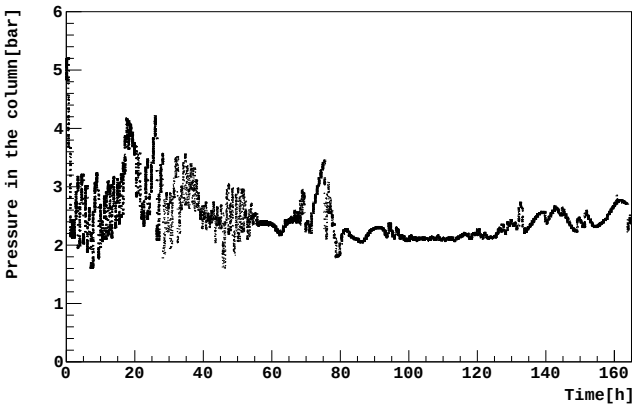

Fig. 12 Measured pressure inside the column in the top vs time, for $^{29}N_2$-$^{28}N_2$ distillation in the prototype plant.

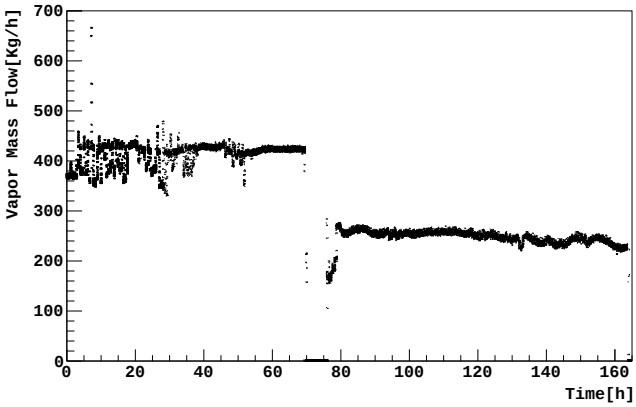

Fig. 11 Measured vapor mass flow in the auxiliary system downstream of the compressor vs time, for $^{29}N_2$-$^{28}N_2$ distillation in the prototype plant.

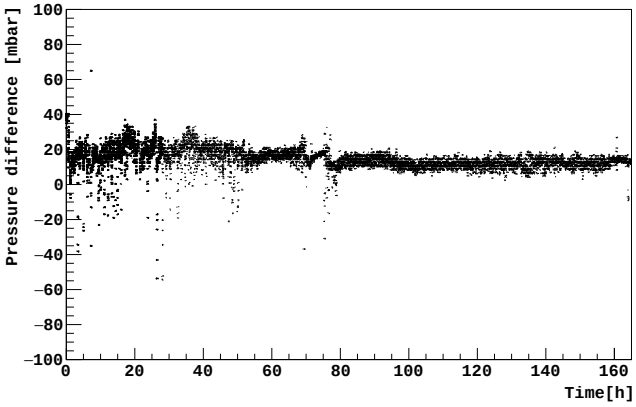

Fig. 13 Measured pressure difference condenser vs. reboiler in the column vs time, for $^{29}N_2$-$^{28}N_2$ distillation in the prototype plant.

the top vs. time. The different pressure in the column compared to what is expected for argon, as discussed in Sect. 3, comes from the different thermodynamic properties of the nitrogen and the operating temperature gradients of the heat exchangers of the reboiler and of the condenser of about 5 K. Since nitrogen was used both for cooling and as distillation fluid, the mass flow rate in the cooling circuit was the same as that inside the column. From Fig. 11 it can be deduced, then, that the mass flowrates during this test ranged between the maximum allowed flow in the column by the packing producer, as discussed in Sect. 4, and half of it. The pressure drop along the prototype column during the second run was of the order of 12 mbar, as shown in Fig. 13. Therefore, for the following calculations, it is possible to assume that both pressure and temperature are constant along the column. The nitrogen temperature inside the column was derived from the pressure measurement using the Antoine equation [15]. From the data of Fig. 12 it follows that, during the second run, the temperature ranged from 83 K to 87 K. The measured vacuum level in the cold box during the two runs was stable around 3×10^{-6} mbar.

6.3 Expected values for nitrogen distillation

The nitrogen molecule, N_2, is mainly formed by two stable isotopes, ^{14}N and ^{15}N, leading to an isotopic fraction of 99.3 % for the $^{28}N_2$ and 0.7 % for the $^{29}N_2$, and, therefore, to an isotopic ratio, R_{N_2}, between the two molecules, of 7.4×10^{-3}. The relative volatility between $^{29}N_2$ and $^{28}N_2$, α_{28-29}, is given, according to [7], by $\ln \alpha_{28-29}$ = 0.846/T - 6.9×10^{-3}, where T is the temperature in Kelvin, implying α_{28-29}=1.003, at the mean column operating temperature of 85 K. This value of the relative volatility is large enough to give a sizeable separation, at total reflux, even with the prototype column that nominally has only about 100 theoretical stages, namely of S^0_{28-29}=1.35.

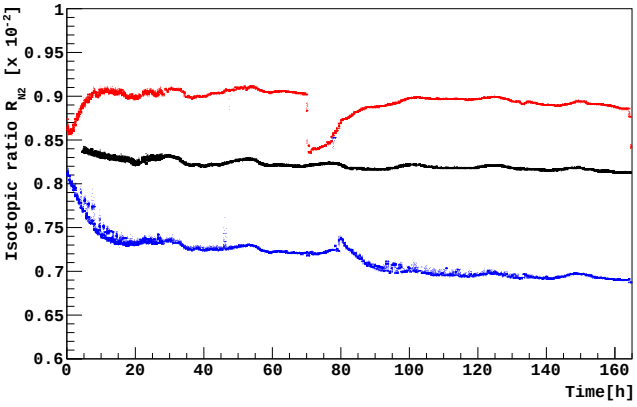

Fig. 14 Reboiler (red), condenser (blue), and feed (black), isotopic ratio R_{N_2} vs. time for $^{29}N_2$-$^{28}N_2$ distillation in the prototype plant.

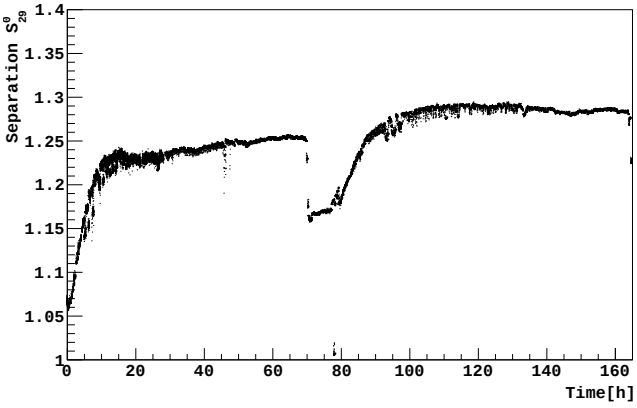

Fig. 15 Separation factor S^0_{28-29} for $^{29}N_2$-$^{28}N_2$ distillation in the prototype plant.

6.4 Distillation measurements

A quadrupole mass spectrometer (Extrel MAX-300) measured the fluid composition, sampling in the reboiler, in the condenser, and in the feed line at the output of the gas bottles, using up to 18 m long and 0.18 mm diameter copper capillaries. With this mass spectrometer, the peaks corresponding to $^{28}N_2$ and $^{29}N_2$ are well separated, and, therefore, isotopic ratio measurements were directly taken from the peak height ratio. In Fig. 14 the measured isotopic ratios R_{N_2} vs. time from the reboiler, condenser and feed are shown. When the plant started operation, the three isotopic ratios were the same. With time, they started to diverge, as expected with the distillation taking place, and, after some time, they reached a plateau value. It should be noticed that at the end of the first run, the isotopic ratio in the reboiler dropped almost to the feed value while the one of the condenser increased only after about 10 h. This is due to the fact that when the compressor and the pumps are switched off, i.e. the distillation process is stopped, the liquid present in the columns sinks quickly in the reboiler under gravity, and mixes with that already present there, whereas this is not the case for the vapor. From Fig. 14 it can also be noticed that the isotopic ratio of the feed gas is not exactly equal to the natural isotopic ratio value discussed in Sect. 6.3 and this is due to the mass spectrometer not fully calibrated before use. Also the isotopic ratio values slightly drifted over time, probably due to some internal component of the spectrometer becoming dirty. Anyhow, the separation, S^0_{28-29}, defined as R_{N_2}(condenser)/R_{N_2}(reboiler), depending only on the ratio of the two R_{N_2}, it is not affected by this drift to first order. Fig. 15 shows the separation, S^0_{28-29}, vs time.

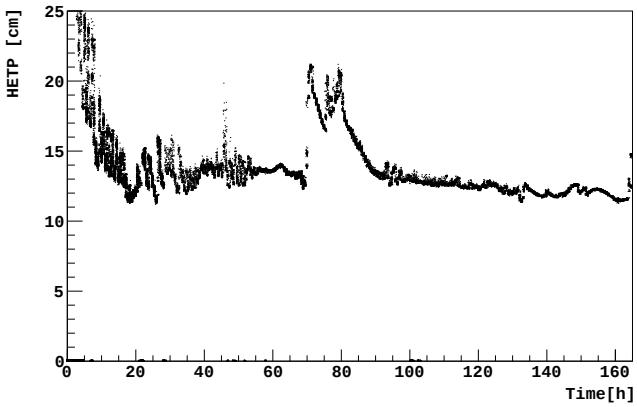

Fig. 16 HETP vs. time for $^{29}N_2$-$^{28}N_2$ distillation in the prototype plant.

6.5 Measurement interpretation

From the measured separation S^0_{28-29} and the calculated relationship between α_{28-29} and temperature, as discussed in Sect. 6.3, it is possible to derive the effective number of theoretical stages and, knowing the packing height per module of 10.24 m, as discussed in Sect. 4, the HETP vs. time, as shown in Fig. 16. The best value obtained during the two runs is about 11.5 cm. This value of HETP is in broad agreement with the assumed value for argon of Sect. 7. This agreement represents a validation of the concept of cryogenic distillation with this plant. However, it should be underlined that the tests described here were performed, in terms of pressure inside the column, outside of the range for which the vendor provides comparison data, and at a value of the sizing parameter F of 0.3 $\sqrt{\text{Pa}}$, which is different from that calculated for argon in Sect. 4. The observed transient, i.e. the time needed to reach plateau operation in Fig. 15, turns out to be about 16 h. It is important to point out that

Table 1 Input parameters of the calculation of ^{39}Ar-^{40}Ar distillation with the McCabe-Thiele method. ρ_L is the liquid argon density at equilibrium at 89.5 K and x_F the molar fraction of ^{39}Ar in the feed. The other parameters are described in the text.

parameter	value
x_F	6×10^{-19}
x_B	6×10^{-20}
α_{39-40}	1.0014
ρ_L	1380 kg/m^3
ρ_V	7.1 kg/m^3
d	31.8 cm
N	2870
$\hat{V}_L$	5 m^3/(h m^2)

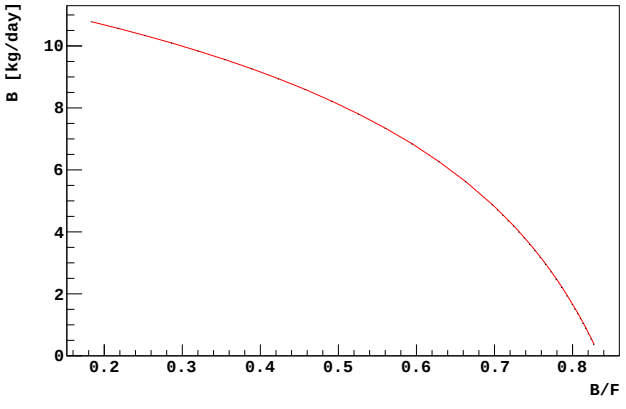

Fig. 17 ^{39}Ar-^{40}Ar distillation with the McCabe-Thiele method: B mass flow vs. B/F.

the time to reach the steady state is strongly dependent on the fluid to be distilled, the duty at the reboiler, and the number of theoretical stages. Further investigation is therefore required before extrapolating this value to the Aria column performance with argon.

7 Projected performance of Aria with argon, at finite reflux

The McCabe-Thiele method was used to calculate the performance of argon distillation in Aria with finite reflux [16]. This method was already applied to cryogenic distillation by collaborations using xenon as active target for dark matter search [8, 10, 11], but it is fair to say that it was never validated with argon. The input parameters of the calculation are summarized in Table 1 and it was also assumed the feed to be a saturated vapor. The relative volatility, α_{39-40}, is assumed constant along the column height and equal to the value corresponding to the mean operating temperature of the column. The calculation was performed for individual values of B/F, where B and F are the mass flow rates in the bottom and feed streams, respectively. Fig. 17 shows B vs. B/F. We consider as benchmark value B/F to be 50 %, a reasonable assumption given the UAr is a valuable material. The McCabe-Thiele diagram corresponding to this benchmark value is shown in Fig. 18. The output parameters of the calculation are shown in Table 2. The calculation also yields the location of the feed point in the column, which turns out to be at the top of the seventh module, i.e. at about 20% height from the top of the column. This is where the feed connections are located. The obtained value of S_{39-40}, the separation of eq. (2) calculated at finite reflux, can be compared with that obtained at total reflux, S^0_{39-40}, which is 57. If x_B were required to be 3×10^{-20}, then B would become 2.5 kg/d, with the same feed point.

Table 2 Output parameters of the calculation of ^{39}Ar-^{40}Ar distillation with the McCabe-Thiele method, for B/F= 50 %. The various parameters are described in the text.

parameter	value
B	8.3 kg/d
F	15 kg/d
R	1547
x_D	1.1×10^{-18}
S_{39-40}	18

The dominant systematic uncertainties in this calculation come from the uncertainty on the mean α_{39-40} value and on the number of theoretical stages, N. As discussed in Sect. 2, α_{39-40} was calculated from the measured value of α_{36-40}. Another publication [17] reports a lower value of α_{36-40} than that reported in Sect. 2, that would lead to α_{39-40}=1.0013 at the mean operating temperature of the column of 89.5 K. At this value one would have a decrease in B by about 25%. A 10% variation on N leads instead to a 30% change in B. Were the measurements of HETP reported in Sect. 6 confirmed in a run with argon, a decrease in B of this magnitude, compared to that of Table 2, could be expected. Eventually, all the output rates are proportional to $\hat{V}_L$, i.e. halving this value leads to halving B. The effect of varying α_{39-40} along the column height according to the temperature profile, was estimated modifying the standard McCabe-Thiele calculation, with the equilibrium curve assumed to be varying stage by stage. A marginal difference in the final result was obtained.

A major assumption in the above calculation is the binary distillation hypothesis, i.e. that isotopes present in the gas other than ^{39}Ar and ^{40}Ar do not influence the calculation. It is well known that ^{36}Ar and ^{38}Ar have sizeable isotopic fractions in AAr, of 0.33% and 0.06%, respectively, though it has been reported that their isotopic fraction is about forty times lower in UAr [18]. However, the assumption of a binary mixture is considered to be reasonable, for two main reasons. On one hand, the two additional isotopes are mostly recovered in the distillate stream, because their relative volatility to ^{40}Ar is larger than one, and therefore we expect no significant difference in the composition of the bottom stream. On the other hand, the isotopic fraction

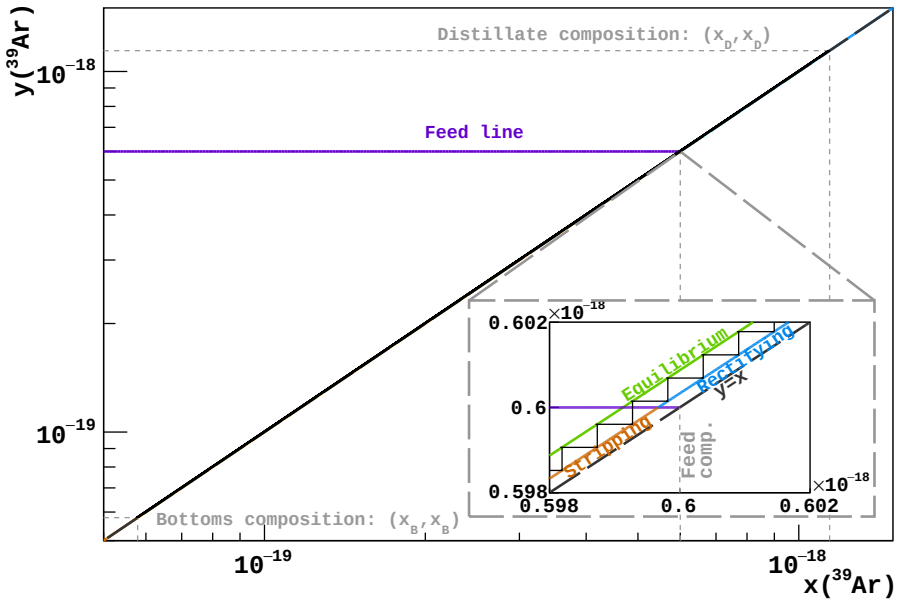

Fig. 18 McCabe-Thiele diagram for the ^{39}Ar-^{40}Ar distillation with the input parameters of Table 1, for B/F= 50 %. The insert is a blow-up of the region indicated by the shaded lines.

of both the distillate and the bottom flow of ^{36}Ar and ^{38}Ar are anyway expected to change only by a small factor since, for each isotope i,

$$\frac{B\cdot(x_B)_i}{F\cdot(x_F)_i}<1 \quad \text{and} \quad \frac{D\cdot(x_D)_i}{F\cdot(x_F)_i}<1 \tag{3}$$

or

$$(x_B)_i<1.8\cdot(x_F)_i \quad \text{and} \quad (x_D)_i<2.2\cdot(x_F)_i, \tag{4}$$

Therefore, the thermodynamic properties of the isotope mixture are marginally changed during the distillation process, and so does α_{39-40}.

Moreover, the presence of ^{36}Ar with a significant isotopic fraction can be very useful for the plant commissioning *e.g.* with atmospheric argon, by measuring isotopic fractions along the column with a mass spectrometer. At total reflux, the separation factor S_{36-40} is 2.8×10^6. At finite reflux, a calculation with the McCabe-Thiele method with the same parameters as above, requiring a reduction factor of 1000, gives the results of Table 3.

Another factor that has to be taken into account, when calculating the plant performance in terms of ^{39}Ar suppression, is the cosmogenic activation of the argon. Cosmogenic activation occurs at the extraction site in Colorado, during transportation, and at the Aria site, during the operation of the plant, since the argon to be processed is stored on the surface. Preliminary studies indicate that the dominant component of the activation comes from cosmic ray neutrons during storage at the Aria site, and is of the order of 15 % of the underground argon radioactivity after distillation, for a 120 d long run to obtain 1 t of argon with a reduced isotopic fraction of 10.

Table 3 McCabe-Thiele method: output parameters for ^{36}Ar-^{40}Ar distillation in a run with atmospheric argon. Feed, F, and bottom, B, mass flowrates of the feed argon, and molar fraction of ^{36}Ar in the top distillate, $(x_D)_{36}$. The calculation was performed requiring the ^{36}Ar isotopic fraction to be reduced by a factor of 1000.

parameter	value
B	45 kg/d
F	60 kg/d
$(x_D)_{36}$	5×10^{-2}

The ^{39}Ar isotopic fraction is so low that it cannot be detected with a mass spectrometer. Therefore, to verify the performance of Aria in terms of isotopic distillation, a new experiment, DArT in ArDM [19], based on a radioactivity measurement, was recently designed and approved at the Canfranc Underground Laboratory (LSC), Spain. The experiment is expected to set an upper limit on the DF, at 90% C.L., of 6×10^{-4}. Therefore, it is expected to measure the residual ^{39}Ar content after distillation in the commissioning phase of the Aria plant with atmospheric argon with good precision.

8 Conclusion and outlook

The design, construction, prototype tests, and performance simulations of the Aria cryogenic distillation column that is currently in the installation phase at Carbosulcis S.p.A., in Nuraxi-Figus (SU), Italy were discussed in detail. The measurement with the prototype of a HETP in broad agreement with the expectations, validated the concept of the cryogenic distillation with this plant. The successful run of the Aria plant is expected to have a tremendous impact in the field of isotopic separation, with applications ranging from nuclear physics to medicine and beyond.

Acknowledgements

The second phase of the leak checks, carried out at CERN, was performed under service agreement KN3155/TE. We acknowledge the professional contribution of the Mine and Electrical Maintenance staff of Carbosulcis S.p.A. Part of the project funding comes from *Intervento finanziato con risorse FSC 2014-2020 - Patto per lo Sviluppo della Regione Sardegna*. This paper is based upon work supported by the U. S. National Science Foundation (NSF) (Grants No. PHY-0919363, No. PHY-1004054, No. PHY-1004072, No. PHY-1242585, No. PHY-1314483, No. PHY- 1314507, associated collaborative grants, No. PHY-1211308, No. PHY-1314501, No. PHY-1455351 and No. PHY-1606912, as well as Major Research Instrumentation Grant No. MRI-1429544), the Italian Istituto Nazionale di Fisica Nucleare (Grants from Italian Ministero dell'Istruzione, Università, e Ricerca "ARIA e la Ricerca della Materia Oscura"- Fondo Integrativo Speciale per la Ricerca (FISR) and Progetto Premiale 2013 and Commissione Scientifica Nazionale II). We acknowledge the financial support by LabEx UnivEarthS (ANR-10-LABX-0023 and ANR-18-IDEX-0001), the Natural Sciences and Engineering Research Council of Canada, SNOLAB, Arthur B. McDonald Canadian Astroparticle Physics Research Institute, the São Paulo Research Foundation (Grant FAPESP-2017/26238-4), and the Russian Science Foundation Grant No. 16-12-10369. The authors were also supported by the "Unidad de Excelencia María de Maeztu: CIEMAT - Física de partículas" (Grant MDM2015-0509), the Polish National Science Centre (Grant No. UMO-2019/33/B/ST2/02884), the Foundation for Polish Science (Grant No. TEAM/2016-2/17), the International Research Agenda Program AstroCeNT - (Grant No. MAB/2018/7) funded by the Foundation for Polish Science from the European Regional Development Fund, the European Union's Horizon 2020 research and innovation program under grant agreement No 962480, the Science and Technology Facilities Council, part of the United Kingdom Research and Innovation, and The Royal Society (United Kingdom). I.F.M.A is supported in part by Conselho Nacional de Desenvolvimento Científico e Tecnológico (CNPq). We also wish to acknowledge the support from Pacific Northwest National Laboratory, which is operated by Battelle for the U.S. Department of Energy under Contract No. DE-AC05-76RL01830.

References

1. P. Agnes, T. Alexander, A.K. Alton, K. Arisaka, H.O. Back, B. Baldin, K. Biery, G. Bonfini, M. Bossa, A. Brigatti et al., Phys. Lett. B **743**, 456 (2015)
2. P. Agnes, L. Agostino, I.F.M. Albuquerque, T. Alexander, A.K. Alton, K. Arisaka, H.O. Back, B. Baldin, K. Biery, G. Bonfini et al., Phys. Rev. D **93**, 081101 (2016)
3. P.A. Amaudruz, M. Baldwin, M. Batygov, B. Beltran, C.E. Bina, D. Bishop, J. Bonatt, G. Boorman, M.G. Boulay, B. Broerman et al., Phys. Rev. Lett. **121**, 071801 (2018)
4. P. Agnes, I.F.M. Albuquerque, T. Alexander, A.K. Alton, G.R. Araujo, D.M. Asner, M. Ave, H.O. Back, B. Baldin, G. Batignani et al., Phys. Rev. Lett. **121**, 081307 (2018)
5. P. Agnes, I.F.M. Albuquerque, T. Alexander, A.K. Alton, G.R. Araujo, D.M. Asner, M. Ave, H.O. Back, B. Baldin, G. Batignani et al., Phys. Rev. Lett. **121**, 111303 (2018)
6. C.E. Aalseth, F. Acerbi, P. Agnes, I.F.M. Albuquerque, T. Alexander, A. Alici, A.K. Alton, P. Antonioli, S. Arcelli, R. Ardito et al., Eur. Phys. J. Plus **133**, 131 (2018)
7. B. Andreev, E. Magomedbekov, A. Raitman, M. Pozenkevich, Y. Sakharovsky, A. Khoroshilov, in *Separation of Isotopes of Biogenic Elements in Two-phase Systems*, edited by B. Andreev, E. Magomedbekov, A. Raitman, M. Pozenkevich, Y. Sakharovsky, A. Khoroshilov (Elsevier, Amsterdam, 2007)
8. Z. Wang, L. Bao, X.H. Hao, Y.L. Ju, K. Pushkin, M. He, J. Instrum. **9**, P11024 (2014)
9. Z. Wang, L. Bao, X. Hao, Y. Ju, Rev. Sci. Instrum. **85**, 015116 (2014)
10. K. Abe, J. Hosaka, T. Iida, M. Ikeda, K. Kobayashi, Y. Koshio, A. Minamino, M. Miura, S. Moriyama, M. Nakahata et al., Astropart. Phys. **31**, 290 (2009)
11. E. Aprile et al. (XENON Collaboration), Eur. Phys. J. C **77**, 275 (2017)
12. R. Fieschi, N. Terzi, Physica **27**, 453 (1961)
13. J.N. Canongia Lopes, A.A.H. Pádua, L.P.N. Rebelo, J. Bigeleisen, J. Chem. Phys. **118**, 5028 (2003)
14. M.R. Fenske, Ind. Eng. Chem. **24**, 482 (1932)
15. M.P. Edejer, G. Thodos, J. Chem. Eng. Data **12**, 206 (1967)
16. W.L. McCabe, E.W. Thiele, Ind. Eng. Chem. **17**, 605 (1925)

17. G. Boato, G. Casanova, M.E. Vallauri, Nuovo Cim. **16**, 505 (1960)
18. R. Saldanha, H. Back, R. Tsang, T. Alexander, S. Elliott, S. Ferrara, E. Mace, C. Overman, M. Zalavadia, Phys. Rev. C **100**, 024608 (2019)
19. C. Aalseth et al. (DarkSide-20k), J. Instrum. **15**, P02024 (2020)

The DarkSide-20k Collaboration

P. Agnes[1], S. Albergo[2,3], I. F. M. Albuquerque[4], T. Alexander[5], A. Alici[6,7], A. K. Alton[8], P. Amaudruz[9], M. Arba[21], P. Arpaia[33], S. Arcelli[6,7], M. Ave[4], I. Ch. Avetissov[10], R. I. Avetisov[10], O. Azzolini[11], H. O. Back[5], Z. Balmforth[12], V. Barbarian[13], A. Barrado Olmedo[14], P. Barrillon[15], A. Basco[16], G. Batignani[17,18], A. Bondar[19,20], W. M. Bonivento[21], E. Borisova[19,20], B. Bottino[22,23], M. G. Boulay[24], G. Buccino[25], S. Bussino[26,27], J. Busto[15], A. Buzulutskov[19,20], M. Cadeddu[28,21], M. Cadoni[28,21], A. Caminata[23], E.V. Canesi[89]*, N. Canci[29], G. Cappello[2,3], M. Caravati[21], M. Cárdenas-Montes[14], N. Cargioli[28,21], M. Carlini[30], F. Carnesecchi[7,6], P. Castello[32,21], A. Castellani[76]*, S. Catalanotti[33,16], V. Cataudella[33,16], P. Cavalcante[29], S. Cavuoti[33,16,35], S. Cebrian[36], J. M. Cela Ruiz[14], B. Celano[16], S. Chashin[13], A. Chepurnov[13], C. Cicalò[21], L. Cifarelli[6,7], D. Cintas[36], F. Coccetti[31], V. Cocco[21], M. Colocci[6,7], E. Conde Vilda[14], L. Consiglio[29], S. Copello[23,22], J. Corning[74], G. Covone[33,16], P. Czudak[37], M. D'Aniello[34], S. D'Auria[38], M. D. Da Rocha Rolo[39], O. Dadoun[40], M. Daniel[14], S. Davini[23], A. De Candia[33,16], S. De Cecco[41,42], A. De Falco[28,21], G. De Filippis[33,16], D. De Gruttola[43,44], G. De Guido[45], G. De Rosa[33,16], M. Della Valle[16,35], G. Dellacasa[39], S. De Pasquale[43,44], A. V. Derbin[46], A. Devoto[28,21], L. Di Noto[23], F. Di Eusanio[52]*, C. Dionisi[41,42], P. Di Stefano[74], G. Dolganov[47], D. Dongiovanni[87]*, F. Dordei[21], M. Downing[48], T. Erjavec[49], S. Falciano[30,41]*, S. Farenzena[88]*, M. Fernandez Diaz[14], C. Filip[86], G. Fiorillo[33,16], A. Franceschi[50], D. Franco[51], E. Frolov[19,20], N. Funicello[43,44], F. Gabriele[29], C. Galbiati[52,29,30], M. Garbini[31,7], P. Garcia Abia[14], A. Gendotti[53], C. Ghiano[29], R. A. Giampaolo[39,54], C. Giganti[40], M. A. Giorgi[18,17], G. K. Giovanetti[55], M.L. Gligan[86], V. Goicoechea Casanueva[56], A. Gola[57,58], A.M. Goretti[29]*, R. Graciani Diaz[59], G. Y. Grigoriev[47], A. Grobov[47,60], M. Gromov[13,61], M. Guan[62], M. Guerzoni[7], M. Guetti[29]*, M. Gulino[63,64], C. Guo[62], B. R. Hackett[5], A. Hallin[65], M. Haranczyk[37], S. Hill[12], S. Horikawa[30,29], F. Hubaut[15], T. Hugues[66], E. V. Hungerford[1], An. Ianni[52,29], V. Ippolito[41], C. C. James[67], C. Jillings[68,69], P. Kachru[30,29], A. A. Kemp[74], C. L. Kendziora[67], G. Keppel[11], A. V. Khomyakov[10], S. Kim[70], A. Kish[56], I. Kochanek[29], K. Kondo[29], G. Korga[12], A. Kubankin[71], R. Kugathasan[39,54], M. Kuss[17], M. Kuźniak[66], M. La Commara[72,16], L. La Delfa[21]*, D. La Grasta[89]*, M. Lai[28,21,51], N. Lami[88]*, S. Langrock[69], M. Leyton[16], X. Li[52], L. Lidey[5], F. Lippi[88]*, M. Lissia[21], G. Longo[33,16], N. Maccioni[88]*, I. N. Machulin[47,60], L. Mapelli[52], A. Marasciulli[18], A. Margotti[7], S. M. Mari[26,27], J. Maricic[56], M. Marinelli[23]*, M. Martínez[36,73], A. D. Martinez Rojas[39,54], A. Martini[88,90]*, C. J. Martoff[70], M. Mascia[85], M. Masetto[89]*, A. Masoni[21], A. Mazzi[57,58], A. B. McDonald[74], J. Mclaughlin[9,12], A. Messina[41,42], P. D. Meyers[52], T. Miletic[56], R. Milincic[56], R. Miola[89]*, A. Moggi[17], A. Moharana[30,29], S. Moioli[45], J. Monroe[12], S. Morisi[33,16], M. Morrocchi[17,18], E. N. Mozhevitina[10], T. Mróz[37], V. N. Muratova[46], A. Murenu[21]*, C. Muscas[32,21], L. Musenich[23,22], P. Musico[23], R. Nania[7], T. Napolitano[50], A. Navrer Agasson[40], M. Nessi[25], I. Nikulin[71], J. Nowak[75], A. Oleinik[71], V. Oleynikov[19,20], L. Pagani[49], M. Pallavicini[22,23], S. Palmas[85], L. Pandola[64], E. Pantic[49], E. Paoloni[17,18], G. Paternoster[57,58], P. A. Pegoraro[32,21], L. A. Pellegrini[45], C. Pellegrino[7], K. Pelczar[37], F. Perotti[76,38], V. Pesudo[14], E. Picciau[28,21], F. Pietropaolo[25], T. Pinna[87]*, A. Pocar[48], P. Podda[88]*, D. M. Poehlmann[49], S. Pordes[67], S. S. Poudel[1], P. Pralavorio[15], D. Price[77], F. Raffaelli[17], F. Ragusa[78,38], A. Ramirez[1], M. Razeti[21], A. Razeto[29], A. L. Renshaw[1], S. Rescia[79], M. Rescigno[41], F. Resnati[25], F. Retiere[9], L. P. Rignanese[7,6], C. Ripoli[44,43], A. Rivetti[39], J. Rode[40,51], L. Romero[14], M. Rossi[23,22], A. Rubbia[53], M. Rucaj[89]*, G.M. Sabiu[88]*, P. Salatino[80,16], O. Samoylov[61], E. Sánchez García[14], E. Sandford[77], S. Sanfilippo[27,26], V.A. Sangiorgio[45], V. Santacroce[88]*, D. Santone[12], R. Santorelli[14], A. Santucci[87], C. Savarese[52], E. Scapparone[7], B. Schlitzer[49], G. Scioli[6,7], D. A. Semenov[46], B. Shaw[9], A. Shchagin[71], A. Sheshukov[61], M. Simeone[80,16], P. Skensved[74], M. D. Skorokhvatov[47,60], O. Smirnov[61], B. Smith[9], A. Sokolov[19,20], R. Stefanizzi[28,21], A. Steri[21], S. Stracka[17], V. Strickland[24], M. Stringer[74], S. Sulis[32,21], Y. Suvorov[33,16,47], A. M. Szelc[77], J.Z. Zsücs-Balázs[86], R. Tartaglia[29], G. Testera[23], T. N. Thorpe[30,29], A. Tonazzo[51], S. Torres-Lara[1], S. Tosti[87]*, A. Tricomi[2,3], M. Tuveri[21], E. V. Unzhakov[46], G. Usai[28,21], T. Vallivilayil John[30,29], S. Vescovi[50]*, T. Viant[53], S. Viel[24], A. Vishneva[61], R. B. Vogelaar[81], M. Wada[66], H. Wang[82], Y. Wang[82], S. Westerdale[21], R. J. Wheadon[39], L. Williams[83], Ma. M. Wojcik[37], Ma. Wojcik[84], X. Xiao[82], C. Yang[62], A. Zani[25], F. Zenobio[89]*, A. Zichichi[6,7], G. Zuzel[37], M. P. Zykova[10]

[1] Department of Physics, University of Houston, Houston, TX 77204, USA
[2] INFN Catania, Catania 95121, Italy
[3] Università of Catania, Catania 95124, Italy
[4] Instituto de Física, Universidade de São Paulo, São Paulo 05508-090, Brazil
[5] Pacific Northwest National Laboratory, Richland, WA 99352, USA
[6] Physics Department, Università degli Studi di Bologna, Bologna 40126, Italy
[7] INFN Bologna, Bologna 40126, Italy
[8] Physics Department, Augustana University, Sioux Falls, SD 57197, USA
[9] TRIUMF, 4004 Wesbrook Mall, Vancouver, BC V6T 2A3, Canada
[10] Mendeleev University of Chemical Technology, Moscow 125047, Russia
[11] INFN Laboratori Nazionali di Legnaro, Legnaro (Padova) 35020, Italy

*Not a member of the DarkSide-20k Collaboration

[12] Department of Physics, Royal Holloway University of London, Egham TW20 0EX, UK
[13] Skobeltsyn Institute of Nuclear Physics, Lomonosov Moscow State University, Moscow 119234, Russia
[14] CIEMAT, Centro de Investigaciones Energéticas, Medioambientales y Tecnológicas, Madrid 28040, Spain
[15] Centre de Physique des Particules de Marseille, Aix Marseille Univ, CNRS/IN2P3, CPPM, Marseille, France
[16] INFN Napoli, Napoli 80126, Italy
[17] INFN Pisa, Pisa 56127, Italy
[18] Physics Department, Università degli Studi di Pisa, Pisa 56127, Italy
[19] Budker Institute of Nuclear Physics, Novosibirsk 630090, Russia
[20] Novosibirsk State University, Novosibirsk 630090, Russia
[21] INFN Cagliari, Cagliari 09042, Italy
[22] Physics Department, Università degli Studi di Genova, Genova 16146, Italy
[23] INFN Genova, Genova 16146, Italy
[24] Department of Physics, Carleton University, Ottawa, ON K1S 5B6, Canada
[25] CERN, European Organization for Nuclear Research 1211 Geneve 23, Switzerland, CERN
[26] INFN Roma Tre, Roma 00146, Italy
[27] Mathematics and Physics Department, Università degli Studi Roma Tre, Roma 00146, Italy
[28] Physics Department, Università degli Studi di Cagliari, Cagliari 09042, Italy
[29] INFN Laboratori Nazionali del Gran Sasso, Assergi (AQ) 67100, Italy
[30] Gran Sasso Science Institute, L'Aquila 67100, Italy
[31] Museo della fisica e Centro studi e Ricerche Enrico Fermi, Roma 00184, Italy
[32] Department of Electrical and Electronic Engineering, Università degli Studi di Cagliari, Cagliari 09123, Italy
[33] Physics Department, Università degli Studi "Federico II" di Napoli, Napoli 80126, Italy
[34] Department of Strutture per l'Ingegneria e l'Architettura, Università degli Studi "Federico II" di Napoli, Napoli 80131, Italy
[35] INAF Osservatorio Astronomico di Capodimonte, 80131 Napoli, Italy
[36] Centro de Astropartículas y Física de Altas Energías, Universidad de Zaragoza, Zaragoza 50009, Spain
[37] M. Smoluchowski Institute of Physics, Jagiellonian University, 30-348 Krakow, Poland
[38] INFN Milano, Milano 20133, Italy
[39] INFN Torino, Torino 10125, Italy
[40] LPNHE, CNRS/IN2P3, Sorbonne Université, Université Paris Diderot, Paris 75252, France
[41] INFN Sezione di Roma, Roma 00185, Italy
[42] Physics Department, Sapienza Università di Roma, Roma 00185, Italy
[43] Physics Department, Università degli Studi di Salerno, Salerno 84084, Italy
[44] INFN Salerno, Salerno 84084, Italy
[45] Chemistry, Materials and Chemical Engineering Department "G. Natta", Politecnico di Milano, Milano 20133, Italy
[46] Saint Petersburg Nuclear Physics Institute, Gatchina 188350, Russia
[47] National Research Centre Kurchatov Institute, Moscow 123182, Russia
[48] Amherst Center for Fundamental Interactions and Physics Department, University of Massachusetts, Amherst, MA 01003, USA
[49] Department of Physics, University of California, Davis, CA 95616, USA
[50] INFN Laboratori Nazionali di Frascati, Frascati 00044, Italy
[51] APC, Université de Paris, CNRS, Astroparticule et Cosmologie, Paris F-75013, France
[52] Physics Department, Princeton University, Princeton, NJ 08544, USA
[53] Institute for Particle Physics, ETH Zürich, Zürich 8093, Switzerland
[54] Department of Electronics and Communications, Politecnico di Torino, Torino 10129, Italy
[55] Williams College, Physics Department, Williamstown, MA 01267 USA
[56] Department of Physics and Astronomy, University of Hawai'i, Honolulu, HI 96822, USA
[57] Fondazione Bruno Kessler, Povo 38123, Italy
[58] Trento Institute for Fundamental Physics and Applications, Povo 38123, Italy
[59] Universiatat de Barcelona, Barcelona E-08028, Catalonia, Spain
[60] National Research Nuclear University MEPhI, Moscow 115409, Russia
[61] Joint Institute for Nuclear Research, Dubna 141980, Russia
[62] Institute of High Energy Physics, Beijing 100049, China

[63] Engineering and Architecture Faculty, Università di Enna Kore, Enna 94100, Italy
[64] INFN Laboratori Nazionali del Sud, Catania 95123, Italy
[65] Department of Physics, University of Alberta, Edmonton, AB T6G 2R3, Canada
[66] AstroCeNT, Nicolaus Copernicus Astronomical Center of the Polish Academy of Sciences, 00-614 Warsaw, Poland
[67] Fermi National Accelerator Laboratory, Batavia, IL 60510, USA
[68] SNOLAB, Lively, ON P3Y 1N2, Canada
[69] Department of Physics and Astronomy, Laurentian University, Sudbury, ON P3E 2C6, Canada
[70] Physics Department, Temple University, Philadelphia, PA 19122, USA
[71] Radiation Physics Laboratory, Belgorod National Research University, Belgorod 308007, Russia
[72] Pharmacy Department, Università degli Studi "Federico II" di Napoli, Napoli 80131, Italy
[73] Fundación ARAID, Universidad de Zaragoza, Zaragoza 50009, Spain
[74] Department of Physics, Engineering Physics and Astronomy, Queen's University, Kingston, ON K7L 3N6, Canada
[75] Physics Department, Lancaster University, Lancaster LA1 4YB, UK
[76] Civil and Environmental Engineering Department, Politecnico di Milano, Milano 20133, Italy
[77] Department of Physics and Astronomy, The University of Manchester, Manchester M13 9PL, UK
[78] Physics Department, Università degli Studi di Milano, Milano 20133, Italy
[79] Brookhaven National Laboratory, Upton, NY 11973, USA
[80] Chemical, Materials, and Industrial Production Engineering Department, Università degli Studi "Federico II" di Napoli, Napoli 80126, Italy
[81] Virginia Tech, Blacksburg, VA 24061, USA
[82] Physics and Astronomy Department, University of California, Los Angeles, CA 90095, USA
[83] Department of Physics and Engineering, Fort Lewis College, Durango, CO 81301, USA
[84] Institute of Applied Radiation Chemistry, Lodz University of Technology, 93-590 Lodz, Poland
[85] Department of Mechanical, Chemical, and Materials Engineering, Università degli Studi, Cagliari 09123, Italy
[86] National Institute for Research and Development of Isotope and Molecular Technologies, Cluj-Napoca 400293, Romania
[87] Department of Fusion and Nuclear Safety Technologies, ENEA, Frascati 00044, Italy
[88] CarboSulcis S.p.A. - Miniera Monte Sinni, Cortoghiana 09010, Italy
[89] Polaris S.r.l., Misinto 20826, Italy
[90] Now at Ministero dello Sviluppo Economico, Palazzo Piacentini, 00187 Roma, Italy